Available online at www.sciencedirect.com
SCIENCE DIRECT®
Journal of Sound and Vibration 271 (2004) 339–363
JOURNAL OF SOUND AND VIBRATION
www.elsevier.com/locate/jsvi

Dynamic characterization of elastomers and identification with rheological models

F. Petrone*, M. Lacagnina, M. Scionti

Dipartimento di Ingegneria Industriale e Meccanica (DIIM), University of Catania, Catania viale A. Doria, 6-95125 Catania, Italy

Received 12 September 2002; accepted 17 February 2003

Abstract

The aim of the present paper is identifying a methodology of study, valid for elastomers in general, in order to experimentally characterize their dynamic behaviour and simulating this behaviour by means of a structured mathematical model. An elastomer was chosen and its equivalent stiffness and equivalent viscous damping coefficient were experimentally determined using a specifically designed test apparatus. The responses to several sinusoidal excitations, characterized by different amplitude and frequency values, were analyzed. Furthermore, different values of static preload applied to the elastomer were considered. The experimental values were reproduced using an equivalent 13 degrees-of-freedom rheological model, optimized through a genetic algorithm.

1. Introduction

In scientific literature, materials with long molecular chains are often referred to as elastomeric polymers. Due to their elevated deformability, damping capacity and wide range of obtainable mechanical properties, they have numerous applications in vibration control. Typically, elastomers show a non-linear elastic and dissipative behaviour. This means that stiffness and damping properties are non-linear functions of the displacement and the velocity of deformation applied to the material. The same non-linear behaviour occurs with respect to frequencies when the elastomers are excited with periodic forces. Furthermore, elastomers have *viscoelastic* dissipative properties highlighted by their mixed behaviour between the purely *elastic* and the purely *viscous* one [1–3].

*Corresponding author. Tel.: +39-095-738-2408; fax: +39-095-330-258.
E-mail addresses: fpetrone@diim.unict.it (F. Petrone), mlacagnina@diim.unict.it (M. Lacagnina), mscionti@diim.unict.it (M. Scionti).

0022-460X/$ - see front matter
doi:10.1016/j.jsv.2003.02.001

A rigorous study of elastomers in the numerous fields of their application is often realized by using a mathematical schematization, which allows the physical behaviour of the material to be analytically simulated. This is achieved by defining models, also known as rheological models, which can be structured in such a way that they reproduce the response of the material to any kind of excitation. In particular, by means of different ways of assembling spring, viscous damping and Coulomb friction sliding elements series or parallel connected, the dynamic equations relating the applied forces, displacements and internal parameters of the rheological model can be calculated [4–6].

In the vibration control area, a simple rheological model used to study the non-linear behaviour of an isolator is presented in [7] where the *jump* phenomenon in the transmissivity coefficient of an elastomer subjected to harmonic forces is discussed. The mathematical model consists of a single-degree-of-freedom mass–spring–damper system where the elastic and dissipative forces are functions of, respectively, displacement and velocity of deformation.

Numerous studies in the field of vibration control have been performed to determine the most appropriate rheological model to simulate the experimental results obtained on elastomer specimens. One approach consists of subjecting an elastomer's specimen to a harmonic load thus determining the resultant hysteresis loop. A mathematical expression is then assumed to relate the strain to the force acting on the system as a function of some unknown parameters. The comparisons of the experimental hysteresis loops with those obtained analytically based on selected mathematical assumption, lead to determine the unknown parameters of the rheological model through a least-squares curve-fitting approach.

An alternative method is based on a comparison of the transmissivity coefficient, in terms of displacement calculated on an experimental single-degree-of-freedom system, where a harmonic force excites the mass at various frequencies. In the corresponding mathematical model, the elastic and dissipative force is imposed as a polynomial of displacement and velocity. Using suitable methodologies to solve the dynamic equation of the obtained non-linear model, the theoretical transmissivity coefficient is determined. Comparing these coefficients with the experimental ones, allows calculating the coefficients of the polynomial previously introduced, then, identifying the rheological model [8].

The present study is based on the first of these two methods. In particular, having designed an appropriate experimental apparatus, a sequence of measurements was defined consisting of exciting the physical system with harmonic signals whose amplitude and frequency were increased in opportune steps. Further, the tests were repeated for three different values of the static preloads applied to the elastomer specimens. In fact, this parameter has a significant influence on the dynamics of the system [9,10].

Next, measuring the contribution of the elastic and the dissipative forces and plotting their overall effect as a function of the displacement undergone by the specimen, experimental hysteresis loops are obtained according to an indirect identification scheme [11,12]. The assessment of these loops provides information regarding the stiffness and the equivalent viscous damping coefficient, considered as fundamental parameters for the dynamic analysis of the material.

In order to mathematically identify the elastomer, several rheological models were defined using linear spring, linear viscous damping and Coulomb friction sliding elements, the latter introduced to guarantee the non-linearity of the system with respect to the displacement applied to the

specimen. Each elementary subsystem is connected to the others in a scheme of series or parallel connections.

Determining the internal parameters of the rheological model represents a critical phase in the identification process. Previous authors have used least-squares methods or parametric identification methods in the frequency domain, adopting the Bouc–Wen mathematical model subjected to harmonic forces [13].

The method proposed in this research makes use of genetic algorithms [14–17]. The experimental data and the harmonic transfer functions of the rheological model are introduced to identify internal parameters of the model. These genetic algorithms are able to minimize the error introduced in the theoretical simulation of the experimental data. The results of this identification process evidence the virtual model's capacity to guarantee trends of the stiffness and viscous damping coefficient comparable with those experimentally obtained, over the entire range of frequencies under investigation.

2. Properties of the elastomers

The typical non-linear trend of the stress–strain curve of a polymer is shown in Fig. 1. This curve is strongly influenced by the geometry of the test specimens, so that, in order to characterize their elastic properties, the hardness of the polymers measured using a *durometer* is usually referenced. Hardness represents an approximate measurement linked to the elastic modulus and independent from the specimen geometry. Besides hardness, other fundamental polymer properties to be mentioned are *resistance to traction*, *maximum elongation* and *compression behaviour*.

Resistance to traction and *maximum elongation* are determined by testing to failure specimens, obtained from suitable vulcanized sheets of the material under examination. The polymer composites commonly used as vibration isolators have a resistance to traction varying from 3500 to 25 000 kPa and a maximum elongation between 150% and 600% of the initial length.

Fig. 2 shows the stress–strain curve of polymer isolators. The area between the load and unload curves represents the hysteresis, which is directly proportional to the damping. Both stiffness and hysteresis depend on the temperature and the velocity at which the specimen is deformed.

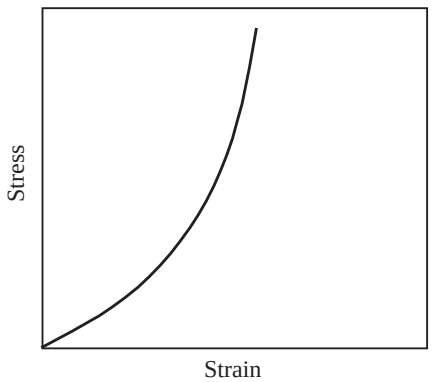

Fig. 1. Typical stress–strain curve of a polymer.

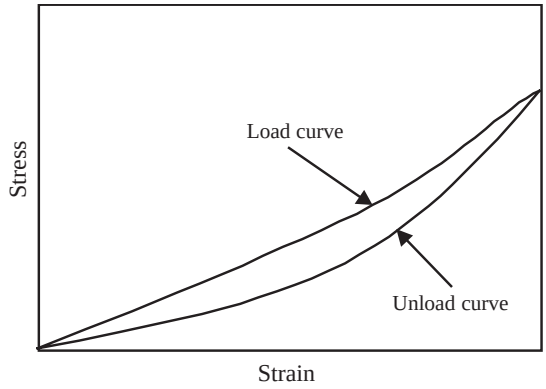

Fig. 2. Stress–strain curve of a polymer isolator.

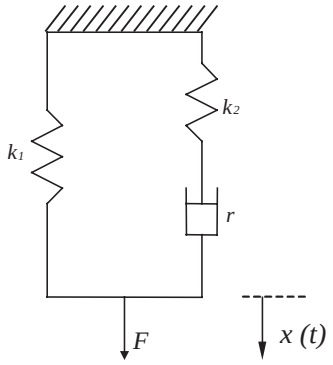

Fig. 3. Zener model for linear viscoelastic analysis.

3. Experimental dynamic identification

3.1. Dynamic behaviour of the elastomers

Polymers do not have a purely elastic behaviour, but exhibit internal damping and their stiffness tends to increase on increasing the frequency of the applied load.

The widest spread mechanical model used to describe the viscoelastic behaviour of these polymers consists of a spring element in parallel with a second spring and a viscous damping element series connected (*Zener model*).

Referring to Fig. 3, if the model is subjected to a sinusoidal force

$$F = F_0 \sin \Omega t, \tag{1}$$

the response is given by

$$x = (F_0/k_1 + k_2)[\sin \Omega t + k_2 \sin \Omega t/k_1(1 + \Omega^2\psi^2) - k_2\Omega\psi \cos \Omega t/k_1(1 + \Omega^2\psi^2)], \tag{2}$$

where

$$\psi = r(1/k_1 + 1/k_2). \tag{3}$$

The first term in brackets in Eq. (2) represents the ordinary elastic response, which is in-phase with the force and independent of the frequency. The second term is also in-phase with the force, but depends on the frequency and represents the elastic component of the viscoelastic response. The third term is responsible for the energy dissipation and it is 90° out-of-phase relatively to the force.

The results of the dynamic analysis of the model are expressed by the *storage modulus* and the *loss modulus*. The storage modulus is proportional to the energy stored and is represented by the first two terms of the expression between brackets in Eq. (2), while the loss modulus is proportional to the energy dissipated and is represented by the third one. Finally, damping is expressed by the relationship

$$\tan\phi = loss\ modulus/storage\ modulus. \tag{4}$$

3.2. Methodology for experimental dynamic identification

To experimentally determine the dynamic characteristics of an elastomer, its response to a periodic excitation at a specified frequency and amplitude and under a given preload must be analyzed, thus determining the corresponding hysteresis loops.

International norms describe the measurement methodology used to determine the dynamic stiffness of isolators, intended as elastic-damping materials. A distinction between two methods is referenced: direct and indirect. In the direct method, the stiffness is calculated using a load cell or a force transducer to measure the force applied straight to the specimen; a displacement transducer or accelerometer occurs to evaluate the resulting displacement. This method has been widely used in the laboratory tests, but presents the drawback that it cannot be used for frequencies above about 200 Hz. The indirect method, where the elastomer under examination is mounted between two rigid masses [18], was therefore chosen for this study. From the measurement of masses accelerations (velocities or displacements), the dynamic stiffness is obtained with no need of evaluating the force applied by the exciter.

An experimental apparatus, preferentially operating in the mass controlled zone, was therefore constructed using piezoelectric accelerometers sensitive to high-frequency accelerations. Such a system, however, is less accurate at low frequencies where accelerations are low unless the excitation amplitudes are high.

In the test apparatus, two sets of four elastomer specimens are placed between an inertial toroidal mass and two circular plates rigidly connected one to another by four bolts. Then, this assembly is screwed on a vibrating shaker. The tightening force of the bolts ensures the preloading of the specimens. Dynamic excitation is supplied by the relative movement of the inertial mass between the two faces of each rubber specimen. To determine the hysteresis loops, from which the dynamic characteristics of the material will be obtained, it is necessary to calculate the relative elastic strain z (undergone by the rubber) and the force required to generate it. Using the notation of Fig. 4, the z value is calculated as the difference between the inertial mass displacement x and the displacement y supplied by the shaker, so that the rubber is subjected to an elongation given by

$$z(t) = x(t) - y(t). \tag{5}$$

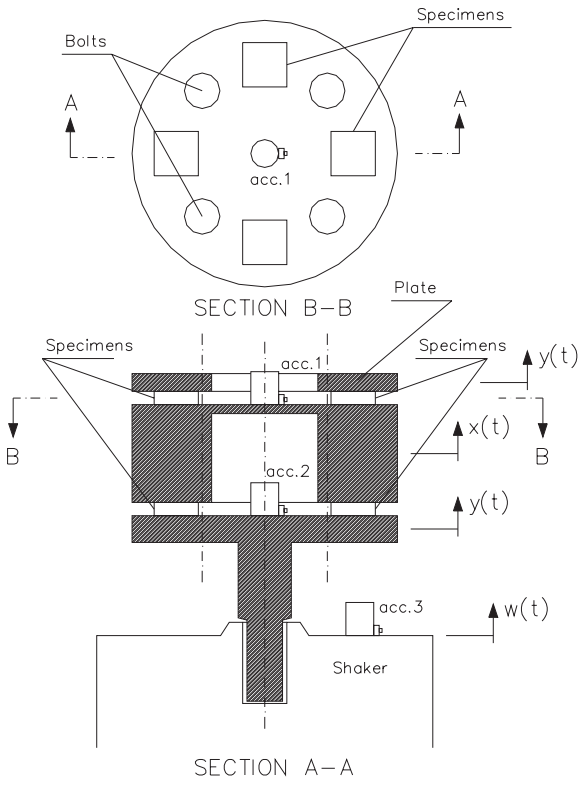

Fig. 4. Section of the experimental apparatus.

To measure any vibrations ($\ddot{w}$) of the body of the shaker on the foundation, a third piezoelectric accelerometer was located on the body of the vibrating shaker. This acceleration can be considered as a measurement noise occurring during the process. The motion equation is given by

$$m\ddot{x} + r_{eq}\dot{z} + k_{eq}z = 0. \tag{6}$$

The reaction force of the rubber, subjected to a displacement z at a velocity $\dot{z}$, is composed by the sum of two terms: the elastic term $k_{eq}z$ (where k_{eq} is the *equivalent dynamic stiffness*) and the viscous term $r_{eq}\dot{z}$ (where r_{eq} represents the *equivalent viscous damping coefficient*).

The parameters k_{eq} and r_{eq} are unknown. However, from Eq. (6) the sum of the elastic and viscous terms, i.e., the reaction force of the rubber, equals the force of inertia ($m\ddot{x}$) of the suspended toroidal mass. This means that, knowing the value of the mass m and measuring its acceleration $\ddot{x}$ by means of an accelerometer placed on it, the reaction force of the rubber can be determined.

3.3. Determination of the field of investigation and the geometry of components

To determine the geometry and mass of the various components of the test apparatus, an operating interval of preloads, amplitudes and excitation frequencies was fixed, taking into account the limits imposed by the available laboratory instruments.

The entire apparatus (Fig. 5) was mounted on the plate of a shaker, so that the overall mass of the system must be limited by the maximum admitted payload of the shaker used for the experiment. The apparatus was, therefore, designed to minimize the masses of the plates, which are in aluminium so that the intermediate exciting mass can be made as large as possible. The system had a total mass of 500 g distributed as follows: 400 g for the steel toroidal mass, 100 g for the two aluminium plates including bolts masses. The mass of the rubber was considered negligible.

The trials were conducted using a B&K 4809 shaker whose optimal operational frequency range is from 100 Hz up to 15 kHz. In general, the dynamic behaviour of the elastomers under examination varies between 0 and 300 Hz, so that the upper limit of the frequency range was set at 300 Hz.

To avoid the occurrence of a dynamic resonance of any component during the experiment, a FEM model, assembled with brick elements, was used to determine the first natural frequencies in free–free and real constraint conditions (Figs. 6 and 7). The numerical results were also verified by an experimental modal analysis using the LMS Cada-X software. The frequencies of the first flexible body modes occur are significantly higher than the maximum operating frequency. The same conclusion was observed for the vibrating modes of the mass, the coupled lower–upper plate system and the whole assembled system so that the upper frequency was validated at 300 Hz. Once determined the total system mass and the frequency upper boundary, the maximum amplitude of transmissible acceleration was set up based on the shaker characteristics. Finally, the lower limits of frequency and acceleration amplitude ranges were fixed.

With the aim of carrying out a process of optimization, the excitation amplitude range, in terms of acceleration of the mass, was set between 1.5 and 4.5 $\boldsymbol{g}$ with a step of 1 $\boldsymbol{g}$ and the frequency range between 40 and 300 Hz.

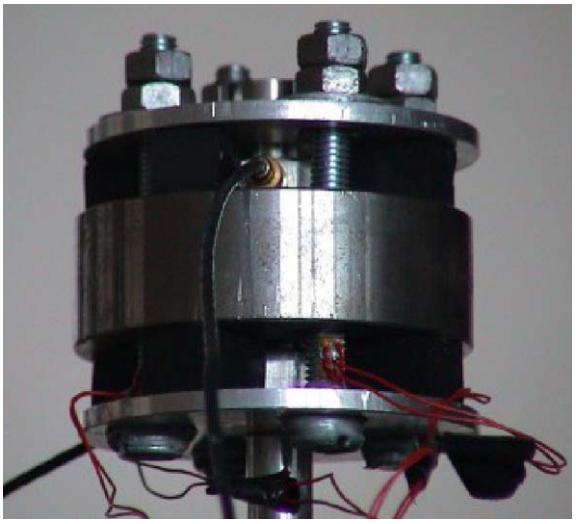

Fig. 5. Experimental apparatus.

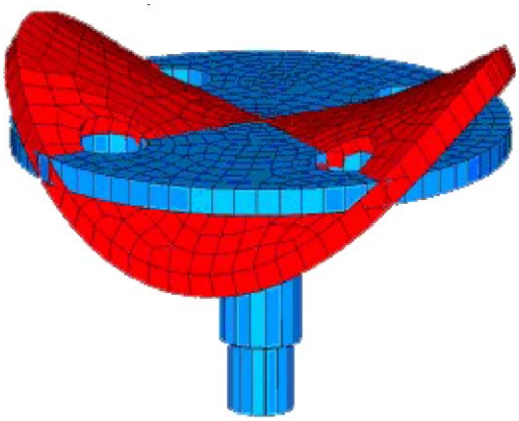

Fig. 6. First mode shape of the free–free lower platform at $f = 4864$ Hz.

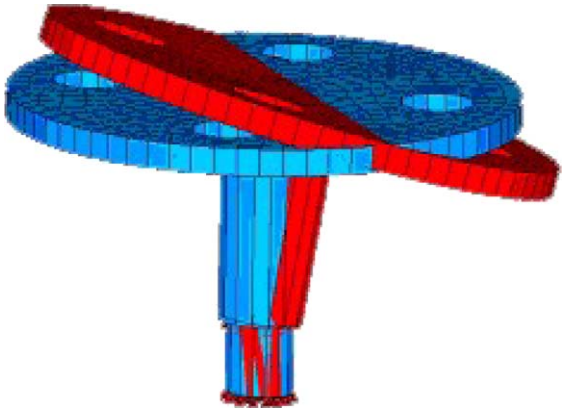

Fig. 7. First mode shape of the constrained lower platform at $f = 1612$ Hz.

3.4. Experimental chain

The employed measurement chain is shown in Fig. 8. In order to obtain consistent experimental data, under different trial conditions, it was decided to run the experimental tests keeping constant the amplitude of the exciting force ($m\ddot{x}$) by means of a control loop where $\ddot{x}$ was constantly monitored according to the scheme shown in Fig. 9.

3.5. Calculation of preload using strain-gauges

The trials on the system were performed with three different preloads which were measured using four electrical resistance axial strain-gauges, each mounted on the lateral surface of the tightening bolts of the two plates (Fig. 10).

Taking into account the dimensions of the specimens, the preload values used in the trials were

$$preload\#1 = 77 \text{ kPa}, \quad preload\#2 = 155 \text{ kPa}, \quad preload\#3 = 232 \text{ kPa}.$$

Fig. 8. Measurement chain.

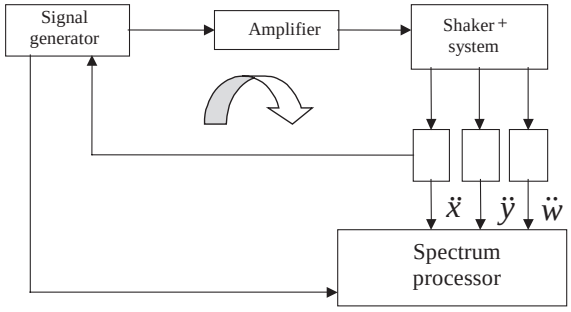

Fig. 9. Block diagram of the measurement chain with feedback loop.

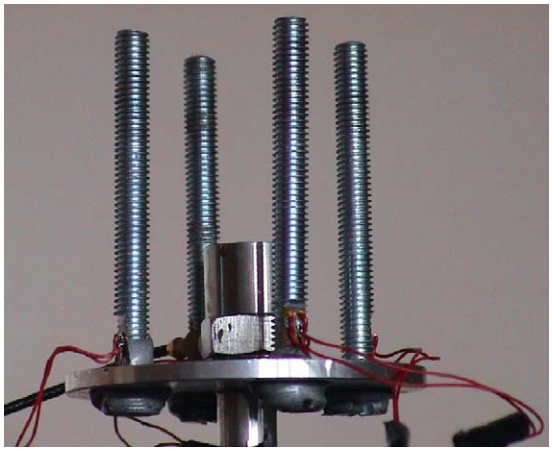

Fig. 10. Detail of the strain-gauges assembly on the bolt surfaces.

In particular, the maximum preload value was chosen so that no disturbances were introduced in the responses as a result of the non-linearity of the stiffness characteristic of the rubber.

4. Analysis of results

The equivalent dynamic stiffness and the equivalent viscous damping coefficient for a given value of frequency, amplitude and acceleration of the toroidal mass and for a given preload, were obtained from the corresponding hysteresis loop.

4.1. Hysteresis loop determination

As an example, Fig. 11 shows the experimental hysteresis curves for a specific trial case. It can be seen that at the lower frequencies the cycles have an irregular profile tending towards an elliptical shape on increasing the test frequency. In the spring-controlled zones, the values of x and y are approximately equal, and consequently the value of z is small and almost indistinguishable from the background noise. In mass-controlled zones, the exciting mass tends to remain stationary and, therefore, the measurement of the relative displacement of the rubber becomes ever more accurate.

4.2. Dynamic stiffness determination

The equivalent dynamic stiffness was determined by calculating the slope, in the plane F-z, of the ideal axis to which the hysteresis loop would be reduced if the damping was zero. In this case,

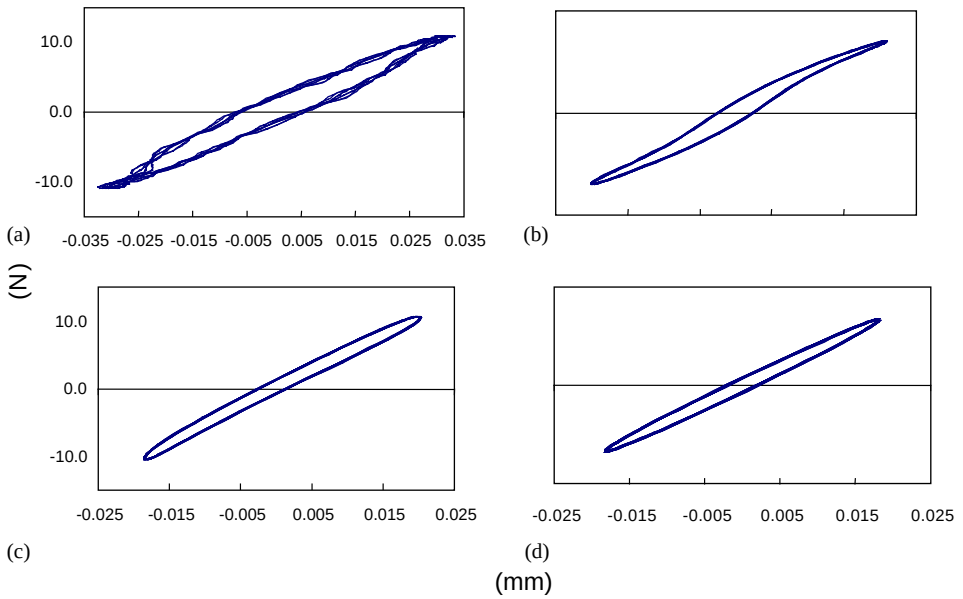

Fig. 11. Hysteresis loops with preload #1 and acceleration amplitude 2.5 $\boldsymbol{g}$ at (a) 40 Hz; (b) 90 Hz; (c) 150 Hz and (d) 300 Hz.

the load–unload cycle is reduced to a segment with the equation

$$F = k_{eq} z, \tag{7}$$

where the equivalent stiffness k_{eq} is the angular coefficient of the straight line with respect to which the inertial moment of the plane figure representing the hysteresis loop is the lowest. The stiffnesses calculated with this method are then plotted as a function of the frequency to highlight the non-linearity of the elastomer's elastic properties versus the frequency.

The dynamic stiffness tends to increase on increasing the frequency and to decrease on increasing the amplitude of the acceleration delivered (Fig. 12). Also, increasing the static preload results in an increase of the equivalent dynamic stiffness (Fig. 13).

The equivalent viscous damping coefficient, r_{eq}, is obtained from the value of dissipated energy, E_d, during a complete load–unload cycle of period $T = 2\pi/\Omega$; it can be expressed by

$$E_d = \int_0^T r_{eq} \dot{z}^2 \, \mathrm{d}t. \tag{8}$$

Thus, the equivalent viscous damping coefficient is given by

$$r_{eq} = E_d / \pi \Omega \dot{z}_0^2, \tag{9}$$

where $\dot{z}_0^2$ represents the maximum amplitude of the velocity strain.

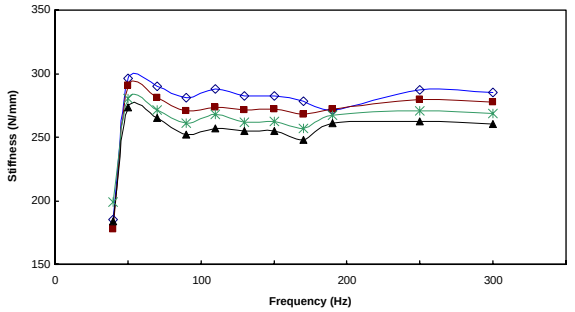

Fig. 12. Variation of the stiffness on a single rubber specimen versus frequency and excitation amplitude at preload #1. Key: –◇–, Acc 1.5 ***g***; –■–, Acc 2.5 ***g***; –✳–, Acc 3.5 ***g***; –▲–, Acc 4.5 ***g***.

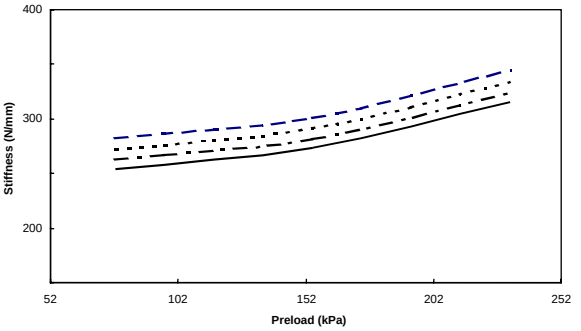

Fig. 13. Variation of the stiffness versus preload and acceleration amplitude at frequency of 150 Hz. Key: (1.5 ***g*** dashed line; 2.5 ***g*** dots line; 3.5 ***g*** dash-dots line; 4.5 ***g*** continuous line).

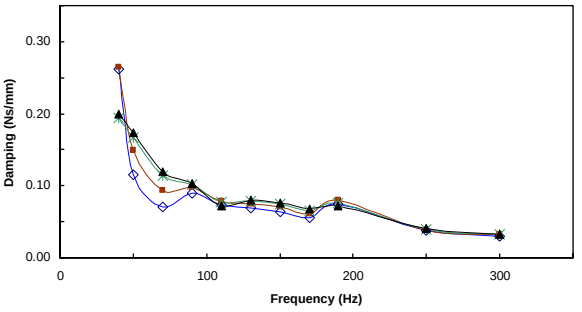

Fig. 14. Variation of the viscous damping coefficient versus excitation amplitude at preload #1. Key: –◇–, Acc 1.5 ***g***; –■–, Acc 2.5 ***g***; –✳–, Acc 3.5 ***g***; –▲–, Acc 4.5 ***g***.

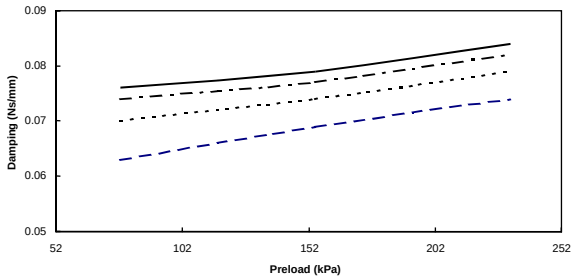

Fig. 15. Variation of the viscous damping coefficient versus preload and acceleration amplitude at frequency of 150 Hz. (1.5 ***g*** dashed line; 2.5 ***g*** dots line; 3.5 ***g*** dash-dots line; 4.5 ***g*** continuous line).

The equivalent viscous damping coefficient tends to decrease on increasing the excitation frequency. On increasing the acceleration amplitude, instead, the coefficient increases, more markedly so, at lower frequencies. Finally, the increase of the static preload for each frequency and amplitude turns into a rise of the coefficient (Figs. 14 and 15).

5. Rheological models

5.1. Introduction to rheological models

The mathematical model used in this study is referred to as rheological model. It can be defined as a proper assembly of elements such as springs, dampers and Coulomb friction sliders which is able to reproduce the viscoelastic characteristics of the real system; therefore, this is a parametric model. In order to select the correct type of elements to be used in the model, some elementary components were first analyzed to assess, for each of them, both the curves of the equivalent viscous damping coefficient and of the equivalent stiffness as functions of the frequency. More complex models were then obtained by the appropriate assembling of the constituent elements on the basis of their characteristics.

5.2. Spring–damper in series element

Two elementary models used to construct more complex models are shown in Figs. 16 and 17. The scheme referred to as Maxwell model consists of a linear spring in series with a linear viscous damper, while the Voigt model has an elastic element and a viscous element in parallel.

Assuming z_0 as the amplitude of the rubber strain, the transfer functions of the two models are represented by Eqs. (10) and (11), respectively as

$$F = z_0(k\Omega^2 r^2/(k^2 + \Omega^2 r^2) + \mathrm{i}\Omega(rk^2/(k^2 + \Omega^2 r^2)))\mathrm{e}^{\mathrm{i}\Omega t}, \tag{10}$$

$$F = z_0(k + \mathrm{i}\Omega r)\mathrm{e}^{\mathrm{i}\Omega t}. \tag{11}$$

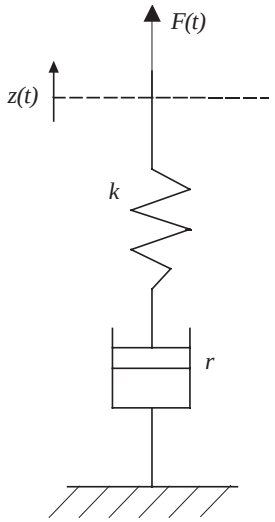

Fig. 16. Model with spring–damper connected in series (Maxwell).

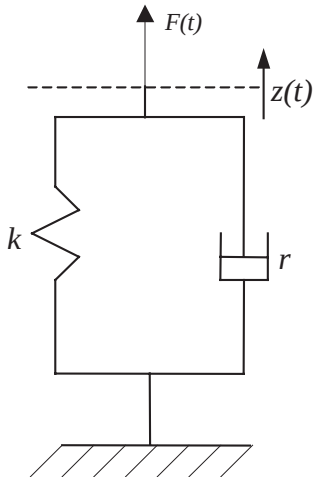

Fig. 17. Model with spring-damper connected in parallel (Voigt).

From Eq. (10), the equivalent stiffness and damping can be obtained for the case of spring and damper in series, respectively as

$$k_{eq} = k\Omega^2 r^2/(k^2 + \Omega^2 r^2), \quad r_{eq} = rk^2/k^2 + \Omega^2 r^2. \tag{12}$$

Analyzing the equivalent dynamic magnitudes with respect to the corresponding static magnitudes (k and r) gives

$$k_{eq}/k = \alpha^2\Omega^2/1 + \alpha^2\Omega^2, \quad r_{eq}/r = 1/(1 + \alpha^2\Omega^2), \tag{13}$$

where

$$\alpha = r/k. \tag{14}$$

Figs. 18 and 19 show the trend of the adimensional magnitudes as a function of the adimensionalized pulse $\bar{\Omega} = \alpha\Omega$. Analyzing the graphs, it can be stated that the Maxwell model is able to simulate an increase in the stiffness on increasing frequency. This element also simulates a decrease in the damping on increasing frequency. From Eq. (13) it is deduced, again, that the amplitude of the displacement delivered influences neither the equivalent stiffness nor the equivalent damping (the element being considered linear).

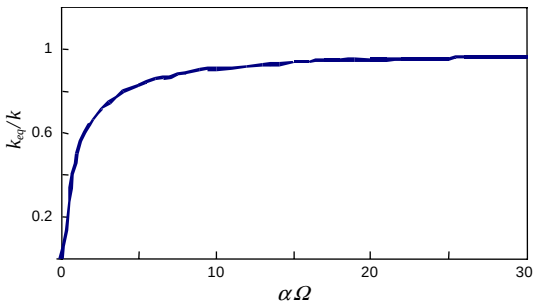

Fig. 18. Variation in equivalent stiffness versus frequency for the Maxwell model.

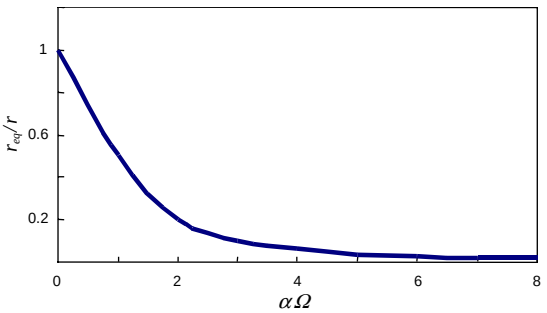

Fig. 19. Variation in equivalent damping versus frequency for Maxwell model.

5.3. Spring–Coulomb friction slider in series element

The element under analysis consists of a linear spring connected in series with a slider that slides over a surface in the presence of Coulomb friction (Fig. 20), where $z(t)$ indicates the displacement applied to the element and F_{fr} the force required to overcome the resistance offered by the friction between the slider and the surface. This element behaves as the slider does not exist until the value of the force caused by the displacement is greater than F_{fr}. Therefore, a displacement amplitude (z_{cr}) above which the slider moves, can be defined as a threshold value given by

$$z_{cr} = F_{fr}/k. \tag{15}$$

Under the assumption that the coefficient of dynamic friction is equal to the static one, once the critical displacement amplitude is exceeded the slider starts to move, avoiding any further force increase. The equivalent stiffness of the element will be, therefore

$$\begin{cases} k_{eq} = k & \text{if } z_0 \leqslant z_{cr}, \\ k_{eq} = F_{fr}/z_0 & \text{if } z_0 > z_{cr}. \end{cases} \tag{16}$$

Fig. 21 shows the qualitative trend of the equivalent stiffness of the spring–slider in series element, as a function of the amplitude of the movement imposed.

The equivalent damping coefficient for a spring–slider in series element can be calculated from Eq. (9) where, in this case:

$$E_d = F_{fr}(z_0 - z_{cr}) = F_{fr}\Delta z_0. \tag{17}$$

Figs. 22 and 23 show the qualitative trends of the equivalent damping, as a function of the displacement amplitude and the frequency.

5.4. Optimization of parameters

To validate the mathematical model, a *genetic algorithm* was used to optimize the parameters of the selected rheological model (stiffness, damping and resistance to friction) in order to simulate

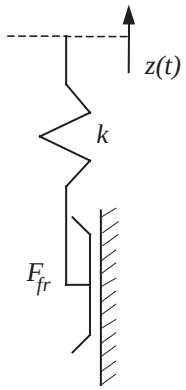

Fig. 20. Spring–Coulomb friction slider connected in series.

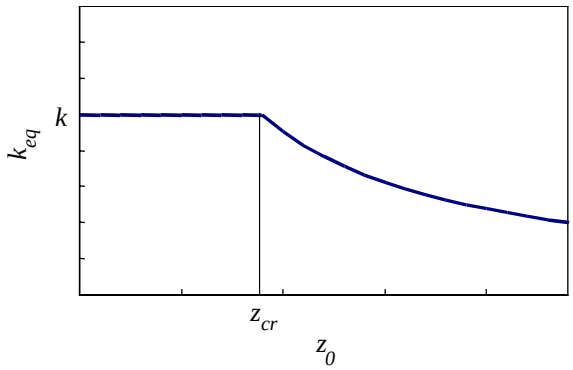

Fig. 21. Equivalent stiffness of spring–Coulomb friction slider connected in series.

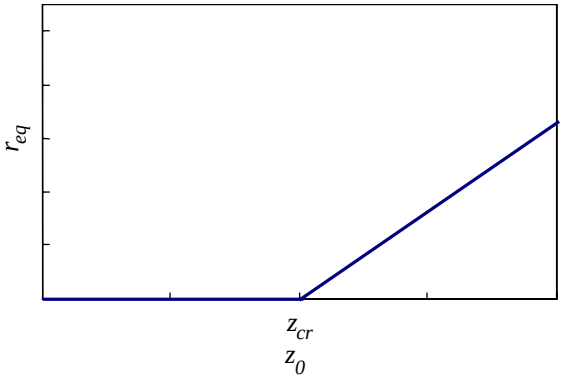

Fig. 22. Equivalent damping coefficient of spring–Coulomb friction slider connected in series.

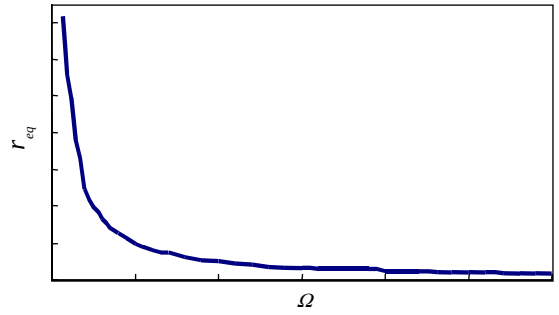

Fig. 23. Variation in the equivalent damping coefficient versus frequency of spring–Coulomb friction slider connected in series.

the real system as accurately as possible. The genetic algorithm provides therefore an index, calculated as the response difference between the rheological model and the real system, which describes the fitness of the model itself.

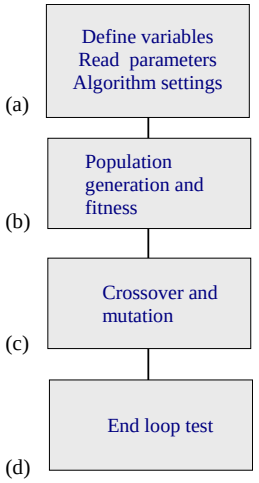

Fig. 24. Genetic algorithm structure.

Beginning with a basic genetic algorithm, written in Fortran code, and with a structure common to most genetic algorithms (Fig. 24) a new algorithm was developed and then adapted, case-by-case, to all the rheological models studied. In particular, a new function was created for the fitness calculation, different subroutines were added for the extraction of the parameters and, finally, files containing the input data were added and modified.

Each of the algorithms used can be represented by four large calculation blocks which perform the following principle functions:

(A) *Statement of all variables*. It should be noted that considerable attention is paid to define the domain (upper and lower boundaries) of the unknowns (internal parameter of the rheological model) used by the algorithm to find the optimum value. This has been provided by means of a preliminary sensitivity analysis, which is not discussed for brevity reasons.

(B) *Generation of an initial population*. It consists of a certain number of individuals, called chromosomes, each in turn composed of a set of parameters, or genes, which characterize the behaviour of the model. The genes of each chromosome are numbers, randomly extracted from an appropriate range, and arranged on a matrix column that, therefore, represents the whole population (Fig. 25). Fitness is a numerical value, which must be proportional to the usefulness or ability of the individual. In the present case, the real output is a sinusoidal alternating force, univocally determined for each frequency from its modulus and phase. Fitness is calculated as the sum of two terms: first, the sum, at the various frequencies, of the absolute values of the differences between the real and rheological modulus; second, the sum, at the various frequencies, of the absolute values of the differences between the real and rheological phases.

Indicating, respectively, the optimal modulus and phases at different frequencies by M_{opt} and φ_{opt} and the rheological modulus and phases at the different frequencies by M_{rhe} and φ_{rhe} and supposing n to be the number of frequencies studied, the fitness is expressed by

$$fitness = \sum_{i=1}^{n} |M_{opt,i} - M_{rhe,i}|/n + \sum_{i=1}^{n} |\varphi_{opt,i} - \varphi_{rhe,i}|/n. \tag{18}$$

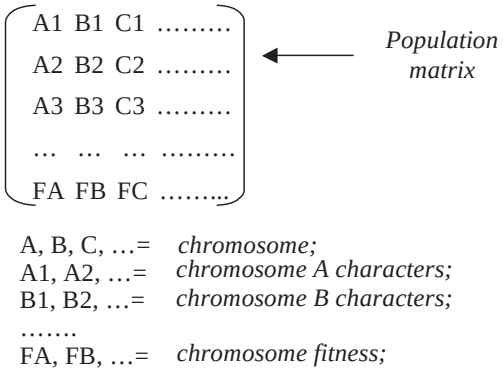

Fig. 25. Structure of population matrix.

Observing that the phase values, expressed in radians, are smaller than the modulus by one or two orders of magnitude, the second term of the sum has a little numerical effect on the total value. Completing the optimization process with a fitness of this type, therefore, presents the risk of introducing significant errors into the simulation of equivalent damping. To avoid this, each term of the second sum was multiplied by an empirical value to give

$$fitness = \sum_{i=1}^{n} |M_{opt,i} - M_{rhe,i}|/n + \sum_{i=1}^{n} 20|\varphi_{opt,i} - \varphi_{rhe,i}|/n. \tag{19}$$

(C) *Reproduction*. It is used to generate successive populations until the optimal solution is reached. Two techniques are used: *crossover* and *mutation*. *Crossover* consists of selecting two individuals, called *parents*, and recombining them to produce two new individuals that become part of the successive generation. The two new individuals generated in this way will take the place of their parents in the next generation only if they are fitter, otherwise they are eliminated. Mutation consists of the entirely random selection of an individual and the substitution of its genes with new genes randomly extracted from a given range. Again, the new individual will substitute its parent in the next generation only if it is fitter.

(D) *Output test*. The process of optimization is interrupted if one of two conditions is met:

(i) the algorithm finds an optimal solution to the given problem, as soon as the fitness of the best individual is lower than a preset value which represents the maximum acceptable error;

(ii) the algorithm does not find an optimal solution to the problem, the number of iterations reaches a preset maximum value and the cycle is interrupted.

6. Complex rheological models

The examined rheological models were obtained by assembling elementary components chosen to simulate the behaviour of the real system. Only those models found to be more reliable, in terms of their ability to simulate the physical phenomenon under investigation, are here reported.

6.1. Model with 11 degrees of freedom

The model with 11 d.o.f. is shown in Fig. 26. It is composed of one ground spring, two spring–damper in series and two spring–slider in series elements. In the case where there is adherence between the slider and the relevant surface, the element behaves as if the slider does not exist. Conversely, in the case where there is movement between the slider and the surface, Eq. (16) states a linear decreasing relation between the equivalent stiffness and the amplitude. For this reason, a constant coefficient $\beta_i > 1$ is introduced as a decreasing factor of the equivalent stiffness so that the contribution of the element to the total reaction force is defined as

$$F_{0i}^{ss} = (k_i/\beta_i)\Delta z_0, \quad i = 3, 5. \tag{20}$$

Fig. 27 shows the trend of the reaction force amplitude of the spring-damper element on varying the amplitude of the displacement imposed. Here, Δz_{cr} represents the amplitude of the critical displacement, above which the amplitude of the reaction force overcomes the resistance offered by the force of friction between the slider and surface and, therefore, sliding begins.

Exciting this model with the displacement $z(t)$ used to excite the real system, the reaction force produced is composed of the sum of five terms due to the contributions of the five elements making up the whole model. The two spring–slider elements behave, therefore, as simple springs in the case of adherence, while they show a decrease in stiffness by a factor β_i in the sliding case.

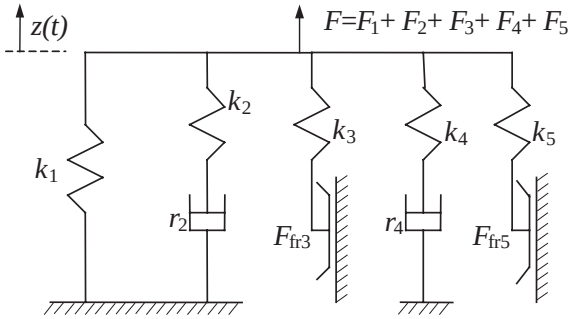

Fig. 26. 11 degrees-of-freedom rheological model.

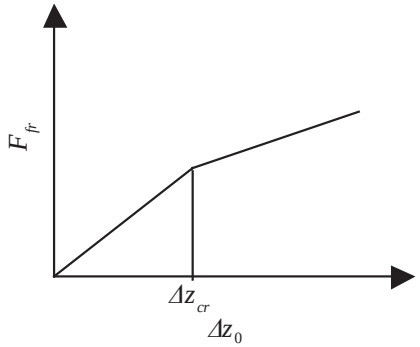

Fig. 27. Force amplitude of the spring–Coulomb friction slider in series model.

Since there are two spring–slider elements, characterized in general by different parameters, the condition of adherence/sliding must be verified on both elements. The total reaction force can therefore have four different expressions according to whether there is adherence on both sliders, sliding on both, or adherence on one and sliding on the other. In fact, the following relations can express the total reaction force:

Adherence–adherence

$$F = \Delta z_0 \left(k_1 + \frac{k_2}{1 + k_2/\mathrm{i}\Omega r_2} + k_3 + \frac{k_4}{1 + k_4/\mathrm{i}\Omega r_4} + k_5 \right) \mathrm{e}^{\mathrm{i}\Omega t}. \tag{21}$$

Sliding–sliding

$$F = \Delta z_0 \left(k_1 + \frac{k_2}{1 + k_2/\mathrm{i}\Omega r_2} + \frac{k_3}{\beta_3} + \frac{k_4}{1 + k_4/\mathrm{i}\Omega r_4} + \frac{k_5}{\beta_5} \right) \mathrm{e}^{\mathrm{i}\Omega t}. \tag{22}$$

Adherence–sliding

$$F = \Delta z_0 \left(k_1 + \frac{k_2}{1 + k_2/\mathrm{i}\Omega r_2} + k_3 + \frac{k_4}{1 + k_4/\mathrm{i}\Omega r_4} + \frac{k_5}{\beta_5} \right) \mathrm{e}^{\mathrm{i}\Omega t}. \tag{23}$$

Sliding–adherence

$$F = \Delta z_0 \left(k_1 + \frac{k_2}{1 + k_2/\mathrm{i}\Omega r_2} + \frac{k_3}{\beta_3} + \frac{k_4}{1 + k_4/\mathrm{i}\Omega r_4} + k_5 \right) \mathrm{e}^{\mathrm{i}\Omega t}. \tag{24}$$

In all four cases, the amplitude and phase of the reaction force can be calculated using the relations

$$F_0 = \sqrt{\mathrm{Re}(F)^2 + \mathrm{Im}(F)^2}, \qquad \varphi = \arctan(-\mathrm{Im}(F)/\mathrm{Re}(F)). \tag{25, 26}$$

After identifying the ranges of variation of the single parameters by a sensitivity analysis and launching the optimization procedure, the results obtained can be plotted and compared with the experimental ones (Figs. 28 and 29). Contrary to that found for stiffness, the results obtained in the simulation of the equivalent viscous damping coefficient (Fig. 29) are more accurate for lower amplitude values and, in any case, show a sharp improvement over models with fewer degrees of freedom.

Finally, the 11 degrees-of-freedom model achieves an excellent degree of precision under all trial conditions. The greatest difference from the real system appears in the simulation of equivalent stiffness at low frequencies and for low acceleration amplitude values.

6.2. *Model with 13 degrees of freedom*

The model with 13 d.o.f. is derived from the previous one, differing from it by a different transfer function characterizing the spring–slider elements. The structure of this model is thus identical to that shown in Fig. 26 for the model with 11 d.o.f.

Analysing the frequency curves experimentally obtained, particularly those of equivalent stiffness, a variation in the values can be seen (an increase in the stiffness and a decrease in the coefficient of viscous damping) in passing from 40 Hz to higher frequencies. The spring–slider elements whose behaviour varies according to the displacement amplitude as well as to frequency

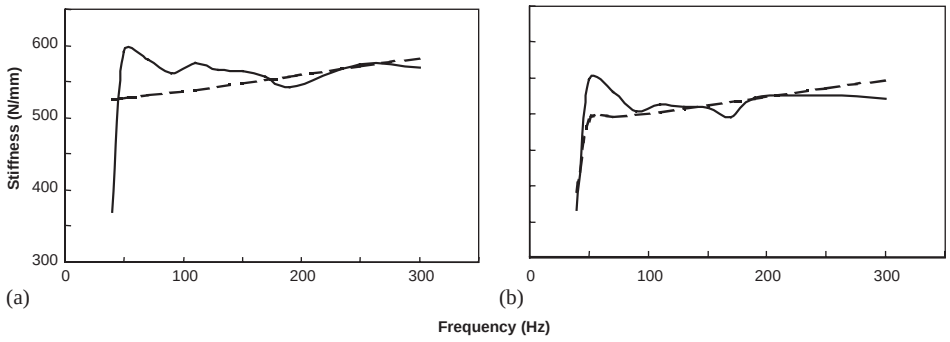

Fig. 28. Comparison of experimental (continuous line) and rheological (dashed line) stiffness for 11 d.o.f. model: (a) acceleration 1.5 $\boldsymbol{g}$ - preload #1; (b) acceleration 4.5 $\boldsymbol{g}$ - preload #1.

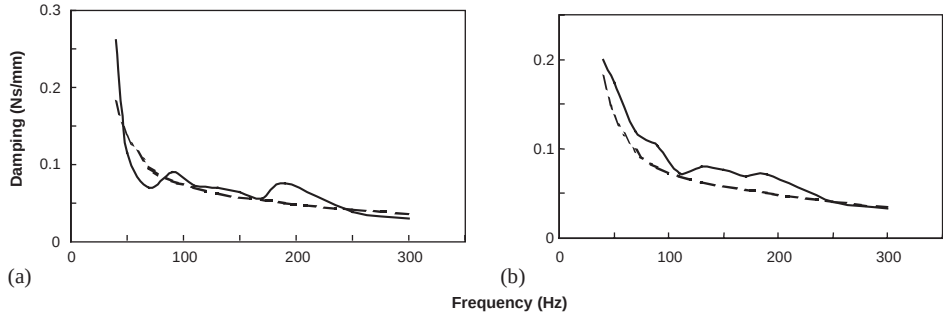

Fig. 29. Comparison of experimental (continuous line) and rheological (dashed line) coefficient of viscous damping for 11 d.o.f. model: (a) acceleration 1.5 $\boldsymbol{g}$, preload #1; (b) acceleration 4.5 $\boldsymbol{g}$, preload #1.

were, therefore, introduced to better approximate the experimental results. To this aim an empirical coefficient $\lambda > 1$ was introduced leading to a new formulation of the reaction force of the spring–slider element. In particular, this reaction force is different according to whether or not the frequency is greater than or equal to 40 Hz. The reaction force amplitude, at a frequency equal to 40 Hz F_{0i}^{ss}, is expressed by the relations:

Adherence

$$F_{0i}^{ss} = (k_i/\lambda_i)\Delta z_0, \tag{27}$$

Sliding

$$F_{0i}^{ss} = (k_i/(\beta_i\lambda_i))\Delta z_0, \tag{28}$$

while for frequencies greater than 40 Hz it becomes

Adherence

$$F_{0i}^{ss} = k_i\Delta z_0, \tag{29}$$

Sliding

$$F_{0i}^{ss} = (k_i/\beta_i)\Delta z_0. \tag{30}$$

From Eqs. (27) and (30) it is clear that the behaviour of the spring–slider elements is identical to that of the previous model at frequencies greater than 40 Hz, while there is a variation in the related transfer function for frequencies equal to 40 Hz through the introduction of the parameter $\lambda_i > 1$ which leads to a reduction in the stiffness independently of the amplitude of displacement.

After a sensitivity analysis as discussed in the previous case, the optimization procedure gave the results shown in Figs. 30 and 31.

The results obtained with the 13 d.o.f. model show a further improvement with respect to the 11 d.o.f. ones and, finally, appear satisfactory under all the trial conditions. Further, on varying the values of the static preload applied to the rubber, curves similar to these were obtained, but are not shown here for brevity reasons. Therefore, the rheological model with 13 d.o.f. can almost exactly reproduce the dynamic characteristics of the real system. Finally, it is worth noting that the optimization procedure was performed three times, that is once for each preload. Thus three sets of ideal model parameters were identified, which, for different preload values, render it similar to the real system.

7. Conclusions

In the present study, a methodology was defined and tested for the experimental identification and analytical simulation of the dynamic behaviour of elastomers.

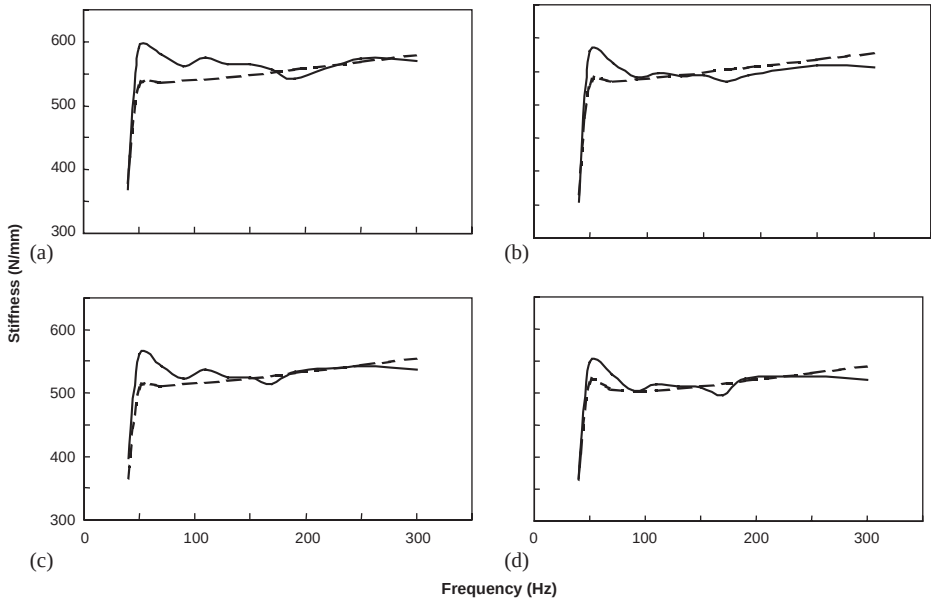

Fig. 30. Comparison of experimental (continuous line) and rheological (dashed line) for 13 d.o.f. model and preload #1: (a) acceleration 1.5 g; (b) acceleration 2.5 g; (c) acceleration 3.5 g; (d) acceleration 4.5 g.

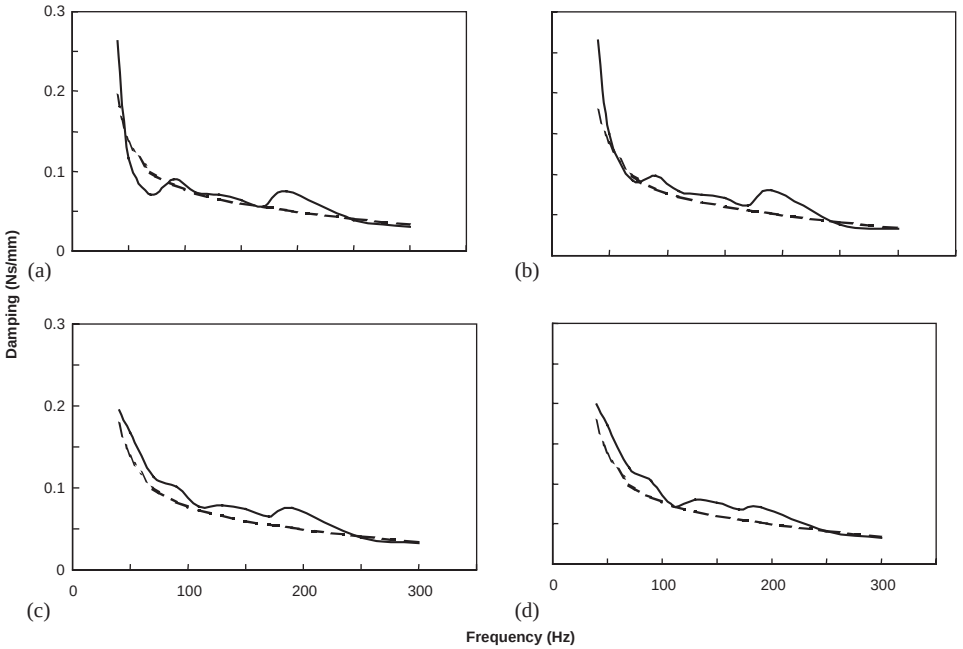

Fig. 31. Comparison of experimental (continuous line) and rheological (dashed line) coefficient of viscous damping for 13 d.o.f. model and preload #1: (a) acceleration 1.5 $\boldsymbol{g}$; (b) acceleration 2.5 $\boldsymbol{g}$; (c) acceleration 3.5 $\boldsymbol{g}$; (d) acceleration 4.5 $\boldsymbol{g}$.

Having designed a suitable apparatus for the experimental trials, the hysteresis loops of the material, subjected to a sinusoidal excitation characterized by different values of amplitude and frequency for given applied static preloads, were analyzed to determine the stiffness and the equivalent viscous damping coefficient.

In particular, the equivalent dynamic stiffness increased on increasing the excitation frequency and the static preload to which the elastomer element was subjected, and decreased on increasing the amplitude of the excitation itself. The coefficient of equivalent viscous damping decreased on increasing the excitation frequency and increased on increasing the acceleration amplitude and the static preload applied.

A rheological model composed of five elements in parallel, each characterized by specific parameters, was therefore determined for each preload applied. These characterizing parameters, allowing the rheological model to generate a response analogous to the experimental behaviour of the real system, were identified using an appropriate genetic algorithm.

With the optimized rheological models, each for a fixed experimental preload, it is possible to simulate with sufficient precision the non-linearities of the physical material. An optimal model was developed, in which the force–displacement law of the Coulomb friction sliders was suitably redefined. Observing that the most significant experimental non-linearities are found in the frequency range 40–50 Hz, a force law was applied to the sliders imposing a decrease in the stiffness of the rheological model in this frequency range.

The simulation of the experimental results was performed on a rheological model with 13 degrees of freedom, able to provide a response analogous to the real system subjected to the same excitations. Finally, comparing the graphs of experimental and simulated stiffness and damping, maximum errors of less than 5% were obtained over the entire frequency range under exam, except for frequencies of 40 Hz where the related error had a mean value of 14% over all the trails performed.

In conclusion, the methodology used was proved valid, both in the experimental identification of the elastomer specimens and in the simulation of their behaviour, and presents opportunities for further developments and improvements, such as, for example, the formulation of a genetic algorithm which also takes account of variation in the preload applied to the rubber. In this case it would be possible to obtain a single rheological model, which simulates the experimental behaviour on varying also this parameter as well as those of the frequency and amplitude of the exciting force.

A further possible application of the methodology described here may lie in the context of finite element virtual simulations. In this sense, laboratory experiment is no longer considered the simple verification of an already developed design, but rather the starting point of a new design that is closer to reality.

References

[1] W.A. Frye, *Handbook of Shock and Vibration*, McGraw-Hill, New York, 1987.
[2] V. Palmov, *Vibrations of Elasto-Plastic Bodies*, Springer, Berlin, 1998.
[3] I.M. Ward, D.W. Hadley, *An Introduction to the Mechanical Properties of Solid Polymers*, Wiley, Chichester, UK, 1993.
[4] M. Berg, A model for rubber springs in the dynamic analysis of rail vehicles, *Proceedings of IMechE*, Vol. 211, Part F, 1997, pp. 95–108.
[5] J. Bastien, M. Schatzmann, C. Lamarque, Study of some rheological models with a finite number of degrees of freedom, *European Journal of Mechanics A/Solids* 19 (2000) 277–307.
[6] M.S. Koval'chenko, Dynamics of uniaxial tension of a viscoelastic strain-hardening body in a system with one degree of freedom. Action of an external force on a compound body, *Strength of Materials* 33 (1) (Part 4) (2001) 125–142.
[7] B. Ravindra, K. Mallik, Performance of non linear vibration isolators under harmonic excitation, *Journal of Sound and Vibration* 170 (3) (1994) 325–337.
[8] A.K. Mallik, V. Kher, M. Puri, H. Hatwal, On the modelling of non-linear elastomeric vibration isolators, *Journal of Sound and Vibration* 219 (2) (1999) 239–253.
[9] J.D. Dickens, Phase velocity of rubber element in vibration isolator under static load, *Journal of Sound and Vibration* 234 (1) (2000) 21–42.
[10] J.D. Dickens, Dynamic model of vibration isolator under static load, *Journal of Sound and Vibration* 236 (2) (2000) 323–337.
[11] UNI EN ISO10846-1:2001.
[12] C.H.M. Richards, R. Singh, Characterization of rubber isolator non linearities in the context of single and multi-degree of freedom experimental system, *Journal of Sound and Vibration* 247 (5) (2001) 807–834.
[13] Y.Q. Ni, J.M. Ko, C.W. Wong, Identification of non linear hysteretic isolators from periodic tests, *Journal of Sound and Vibration* 217 (4) (1998) 737–756.
[14] G. Celano, A. Costa, S. Fichera, Heuristic algorithms for the optimisation of mixed model assembly lines, CD-ROM of the *Proceedings of 16th International Conference on Production Research*, paper I6.3, 2001.
[15] L. Davis, *Handbook of Genetic Algorithms*, Van Nostrand Reinhold, New York, 1991.

[16] D.E. Goldberg, *Genetic Algorithms in Search, Optimization and Machine Learning*, Addison-Wesley, New York, 1989.
[17] Z. Michalewicz, *Genetic Algorithms + Data Structures = Evolution Program*, Springer, New York, 1994, ISBN 3-540-58090-5.
[18] D.J. Thomson, Development of the indirect method for measuring the high frequency dynamic stiffness of resilient elements, *Journal of Sound and Vibration* 213 (1) (1998) 169–188.